Supplementary Information

Supplementary Figures

Figure S1. Docking results according to scoring functions (Chemscore and ChemPLP) and a function term (ChemScore's ΔG). Charts representing boxplots for Chemscore, ΔG, and ChemPLP values of the **(a)** control, **(b)** natural) and **(c)** synthetic compounds under study. For a given chart, each dot in a box plot represents a score for a compound in a docking condition, varying by RBD-containing structure, absence or presence of mutation, and according to region. Outliers beyond the range shown in the charts were omitted.

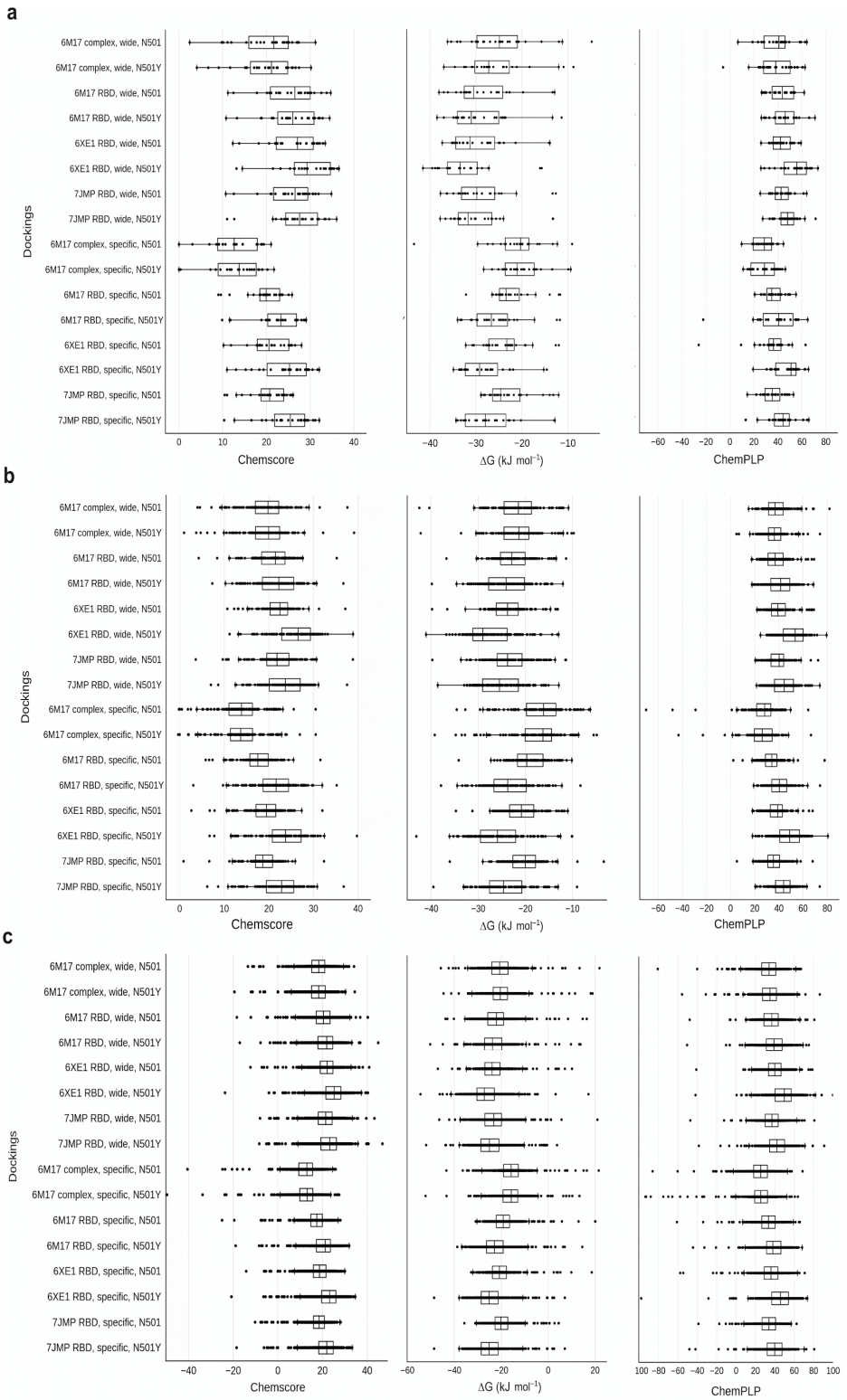

Figure S2. Correlation matrices between the functions and their terms employed to evaluate the docking results of the wide region. Correlation matrices for control (a-d), natural (e-h), and synthetic (i-l) compounds docked with N501 (a, b, e, f, i, j) and N501Y (c, d, g, h, k, l) RBD-containing structures, applying Pearson's (a, c, e, g, i, k) and Spearman's coefficients (b, d, f, h, j, l) to the mean results of each compound docked in the wide region. Chemscore function used for scoring is composed of the following terms: ΔG (binding energy), H bond (score for hydrogen bonds), Lipo. (protein-ligand lipophilic term contribution), H rot. (ligand conformational entropy loss when binding to the protein), Int. H bond (internal H bond, ligand intramolecular H bond contribution), DE clash (protein-ligand steric hindrance), DE int. (internal ligand torsional strain penalty), Int. cor. (internal ligand energy offset). ChemPLP used for rescoring presents an RMSD term (root mean square deviation between all conformations run for a ligand).

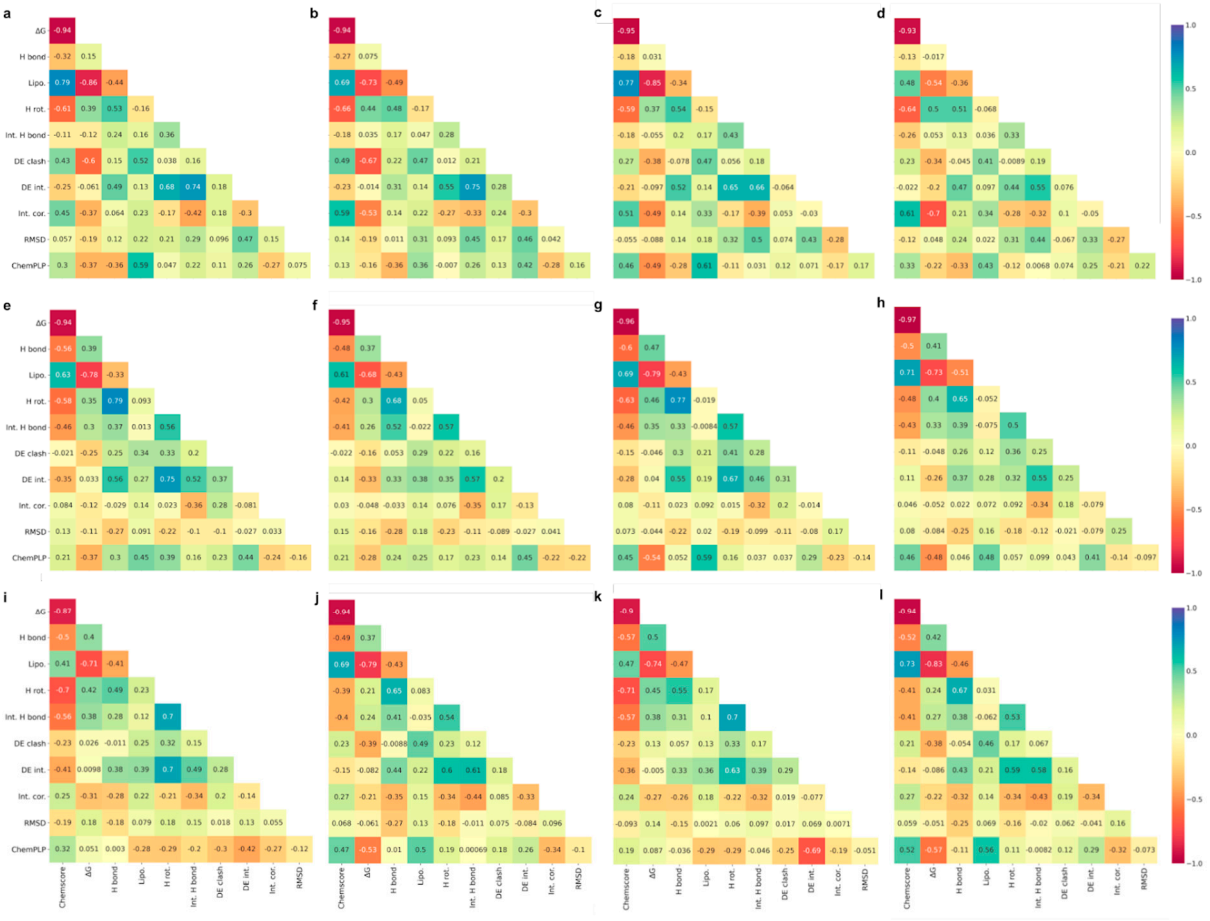

Figure. S3. Correlation matrices between ADME-related properties, the main functions, and terms used to evaluate the docking results of the wide region. Correlation matrices for control (a-b), natural (c-e), and synthetic (e-f) compounds, applying Pearson's (a, c, e) and Spearman's (b, d, f) coefficients. Each chart shows ADME-related properties, calculated from SwissADME, alongside Chemscore, ΔG, and ChemPLP mean results of each compound docked in the wide region of N501 and N501Y (indicated by an asterisk) RBD-containing structures.

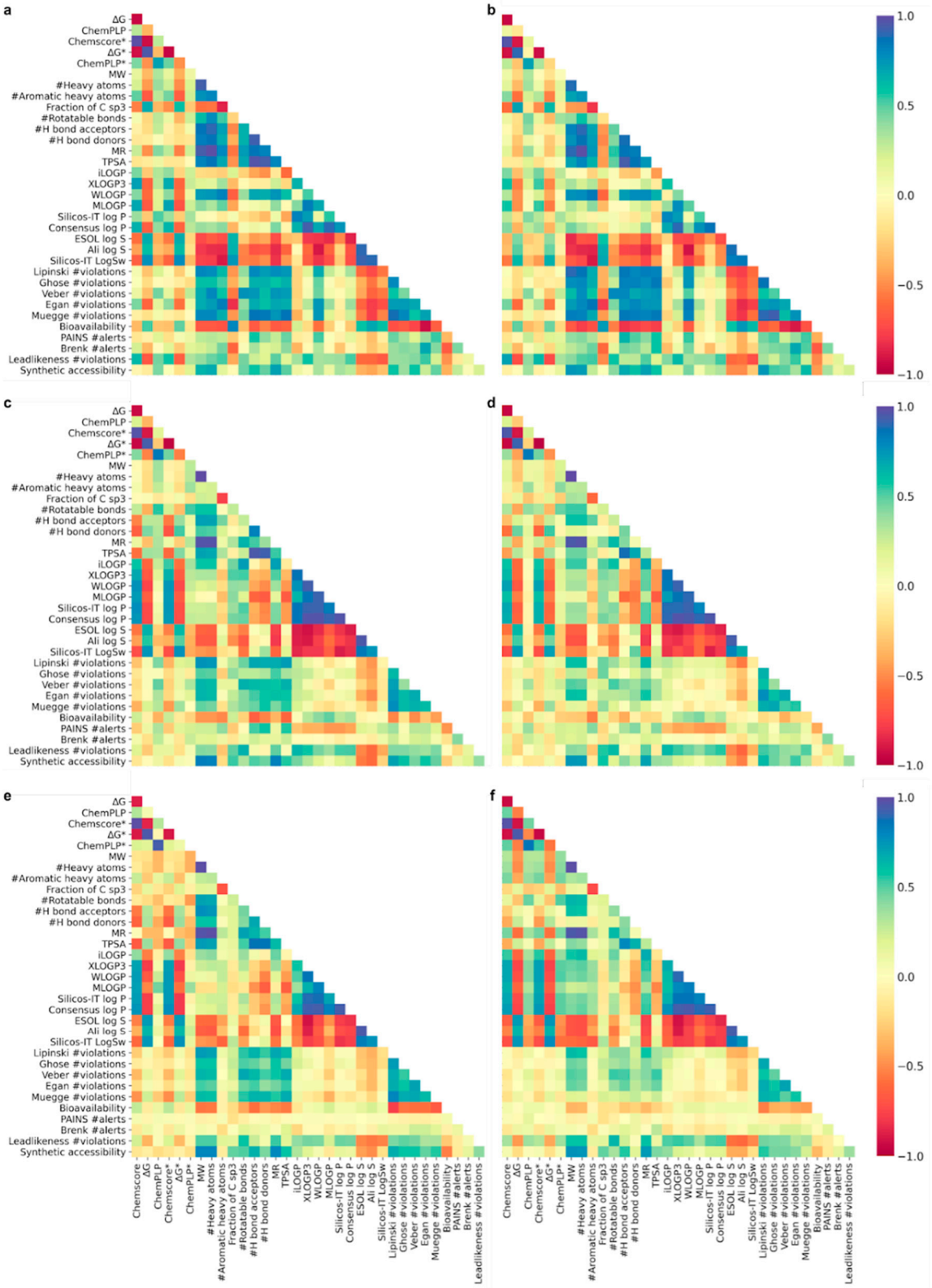

Figure S4. Interaction networks of the most frequent residues interacting with the top 10 hits. Interaction networks of the most frequent residues from N501 (upper left) and N501Y (lower left) RBD-containing structures interacting with the top 10 hits. The charts on the left only considered RBD residues from 6M17 RBD-ACE2, 6M17, 6XE1, and 7JMP RBDs. On the right, the most frequent RBD and ACE2 residues from 6M17 RBD-ACE2 interacting with the top 10 hits.

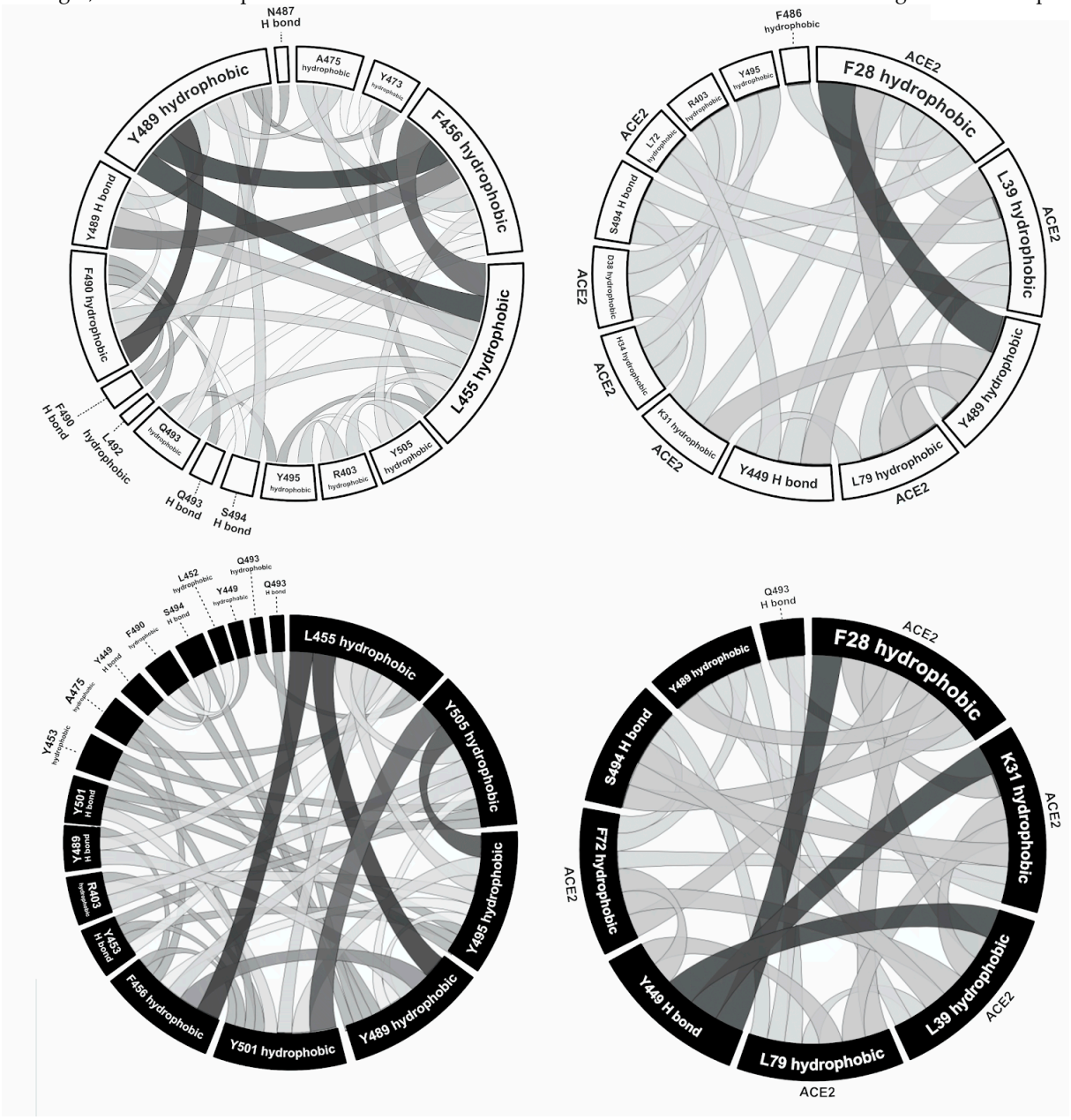

Figure S5. Interaction profile between N501 or N501Y RBDs with ACE2. Nested pie charts of RBD (left chart) and ACE2 (right chart) interactions with the hits. White indicates N501 RBDs; black, N501Y. RBD interactions found less than six times were not exhibited in the figure, but aggregated in the "Other" categories. They are the following: forming H bonds, Y505 (4), F456 (3), K417 (3), N501 (3), G502 (2), E484 (2), Q498 (1), A475 (1), G447 (1) and Y495 (1) (N501 RBDs); N487 (5), G502 (5), F490 (3), Y505 (3), Q498 (3), T500 (3), G446 (2), L492 (2), G496 (2), F456 (1), A475 (1), E484 (1), Y495 (1), G447 (1) and F497 (1) (N501Y RBDs); hydrophobic contacts: Y449 (4), F497 (4), E484 (3), Y421 (2), Y453 (2), K417 (1), N487 (1), Y351 (1), K458 (1), I472 (1), G485 V483 and G496 (1) (N501 RBDs); L492 (5), F497 (5), K417 (4), Y473 (2), E484 (2), Y421 (2), F486 (1), N487 (1), K444 (1), S494 (1), P499 (1), T500 (1), G502 (1) and G504 (1) (N501Y RBDs). The data considered protein-ligand interactions between the hits and 6M17 complex, 6M17, 6XE1, and 7JMP RBDs in N501 and N501Y versions.

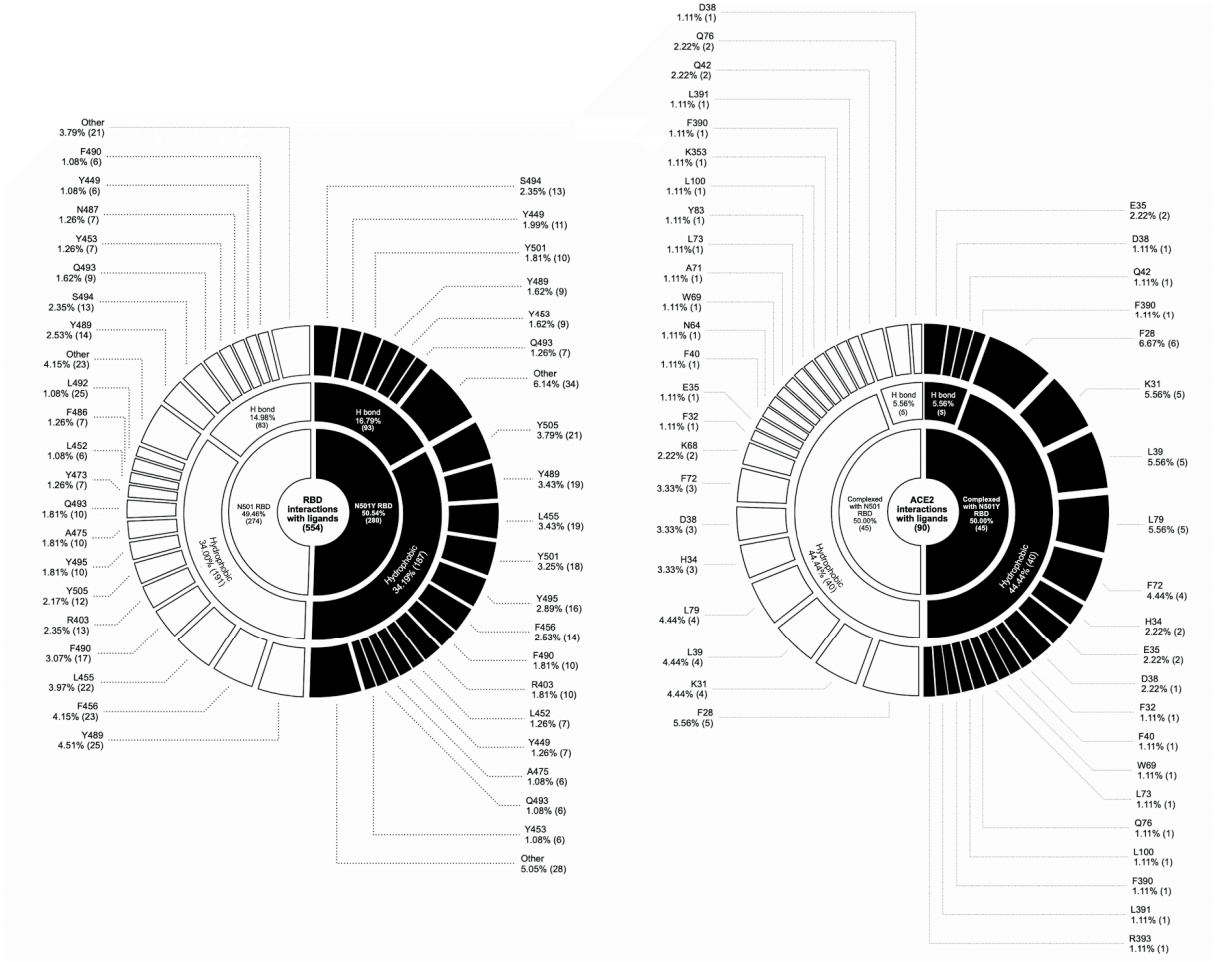

Figure S6. PDBePISA's main results for RBD sequences from RBD-ACE2 complexes. The figure highlights certain interfacing (yellow), solvent-accessible (light blue), and inaccessible residues (dark blue). HSDC, residues making hydrogen/disulfide bond, salt bridge or covalent link; ASA, accessible surface area [Å2]; BSA, buried surface area [Å2]; ΔiG, solvation energy effect [kcal mol–1]; ||||, buried area percentage, one bar per 10%.

N501 RBD	HSDC	ASA	BSA	Δ^iG
E:VAL 401		0.12	0.00	0.00
E:ILE 402		0.00	0.00	0.00
E:ARG 403		77.37	26.57 ||||	-0.59
E:GLY 404		8.08	0.00	0.00
E:GLY 416		20.00	0.00	0.00
E:LYS 417		92.54	15.42 ||	0.07
E:ILE 418		1.06	0.00	0.00
E:LYS 444		113.80	0.00	0.00
E:VAL 445		138.87	5.93 |	-0.01
E:GLY 446		77.07	5.99 |	-0.07
E:GLY 447		15.17	0.00	0.00
E:ASN 448		6.92	0.00	0.00
E:TYR 449	H	143.57	36.04 |||	-0.29
E:ASN 450		115.76	0.00	0.00
E:TYR 451		13.01	0.00	0.00
E:LEU 452		53.97	0.00	0.00
E:TYR 453		35.14	24.95 |||||||	-0.24
E:ARG 454		6.43	0.00	0.00
E:LEU 455		50.71	50.46 |||||||||	0.15
E:PHE 456		55.09	43.80 |||||||	0.57
E:ARG 457		51.48	0.00	0.00
E:ILE 472		50.93	0.00	0.00
E:TYR 473		60.77	17.68 |||	-0.05
E:GLN 474		79.19	0.00	0.00
E:ALA 475		26.61	19.57 |||||||	0.31
E:GLY 476		60.10	29.55 |||||	0.29
E:SER 477		139.78	0.00	0.00
E:GLU 484		41.59	0.00	0.00
E:GLY 485		55.46	9.03 ||	-0.09
E:PHE 486		178.44	97.32 ||||||	1.08
E:ASN 487		61.20	47.39 |||||||	-0.23
E:CYS 488		1.33	0.00	0.00
E:TYR 489	H	93.57	80.93 ||||||||	0.15
E:PHE 490		93.51	0.48 |	0.00
E:PRO 491		3.17	0.00	0.00
E:LEU 492		19.54	0.00	0.00
E:GLN 493	H	78.08	66.16 ||||||||	-0.18
E:SER 494		49.60	4.42 |	-0.05
E:TYR 495		37.81	17.36 |||||	-0.20
E:GLY 496	H	20.37	15.63 |||||||	0.00
E:PHE 497		3.74	0.00	0.00
E:GLN 498		74.80	72.18 |||||||||	-0.64
E:PRO 499		57.94	0.00	0.00
E:THR 500	H	111.20	89.36 ||||||||	0.40
E:ASN 501	H	45.37	36.76 ||||||||	-0.13
E:GLY 502	H	43.11	39.25 |||||||||	0.27
E:VAL 503		120.97	29.08 |||	0.02
E:GLY 504		32.63	1.46 |	0.00
E:TYR 505	H	110.62	78.46 |||||||	0.47
E:GLN 506		23.54	0.00	0.00
E:PRO 507		0.00	0.00	0.00
E:TYR 508		30.59	0.00	0.00

N501Y RBD	HSDC	ASA	BSA	Δ^iG
E:VAL 401		0.41	0.00	0.00
E:ILE 402		0.50	0.00	0.00
E:ARG 403		77.37	17.46 |||	-0.32
E:GLY 404		8.08	0.00	0.00
E:GLY 416		28.65	0.00	0.00
E:LYS 417		84.79	6.92 |	-0.06
E:ILE 418		5.48	0.00	0.00
E:LYS 444		124.37	0.00	0.00
E:VAL 445		127.47	1.23 |	-0.01
E:GLY 446		72.03	4.03 |	-0.05
E:GLY 447		14.98	0.00	0.00
E:ASN 448		14.76	0.00	0.00
E:TYR 449	H	130.19	30.86 |||	-0.26
E:ASN 450		116.65	0.00	0.00
E:TYR 451		19.03	0.00	0.00
E:LEU 452		46.35	0.00	0.00
E:TYR 453		36.07	22.54 ||||||	-0.25
E:ARG 454		11.57	0.00	0.00
E:LEU 455		39.34	38.09 |||||||||	0.61
E:PHE 456		63.10	48.12 |||||||	0.77
E:ARG 457		56.59	0.00	0.00
E:ILE 472		54.85	0.00	0.00
E:TYR 473		64.52	14.02 |||	0.05
E:GLN 474		85.71	0.00	0.00
E:ALA 475		42.18	25.10 |||||	0.40
E:GLY 476		50.38	22.46 |||||	0.29
E:SER 477		121.57	0.00	0.00
E:GLU 484		47.99	0.00	0.00
E:GLY 485		61.33	6.30 ||	-0.07
E:PHE 486		171.02	77.98 |||||	1.25
E:ASN 487		49.72	31.06 ||||||	-0.26
E:CYS 488		2.98	0.00	0.00
E:TYR 489	H	104.13	82.98 |||||||	0.44
E:PHE 490		90.61	1.91 |	0.01
E:PRO 491		3.49	0.00	0.00
E:LEU 492		25.70	0.00	0.00
E:GLN 493	H	83.52	61.87 |||||||	-0.45
E:SER 494		48.40	0.00	0.00
E:TYR 495		38.45	13.79 ||||	-0.16
E:GLY 496	H	10.38	6.09 |||||	0.05
E:PHE 497		4.99	0.00	0.00
E:GLN 498		57.10	51.70 |||||||||	-0.63
E:PRO 499		55.31	0.00	0.00
E:THR 500	H	120.69	84.38 |||||||	0.29
E:TYR 501		72.19	65.00 |||||||||	0.31
E:GLY 502	H	48.14	36.43 |||||||	0.30
E:VAL 503		108.11	13.68 ||	0.12
E:GLY 504		26.78	0.00	0.00
E:TYR 505	H	112.78	74.87 |||||||	0.53
E:GLN 506		26.77	0.00	0.00
E:PRO 507		1.65	0.00	0.00
E:TYR 508		28.18	0.00	0.00

Figure S7. Comparison between N501 and N501Y RBDs in complex with ACE2. a) Estimation, from the PRODIGY server, of the free energy changes and dissociation constants for N501 and N501Y RBD-ACE2. b) Estimation by PRODIGY of the number of interfacial contacts in N501 and N501Y RBD-ACE2. In this server, the default threshold distance for the number of intermolecular contacts at the interface is 5.5 Å. c) Results from the HyPPI Prediction server (proportions of transient complexes to crystal artifacts for N501 and N501Y RBD-ACE2)

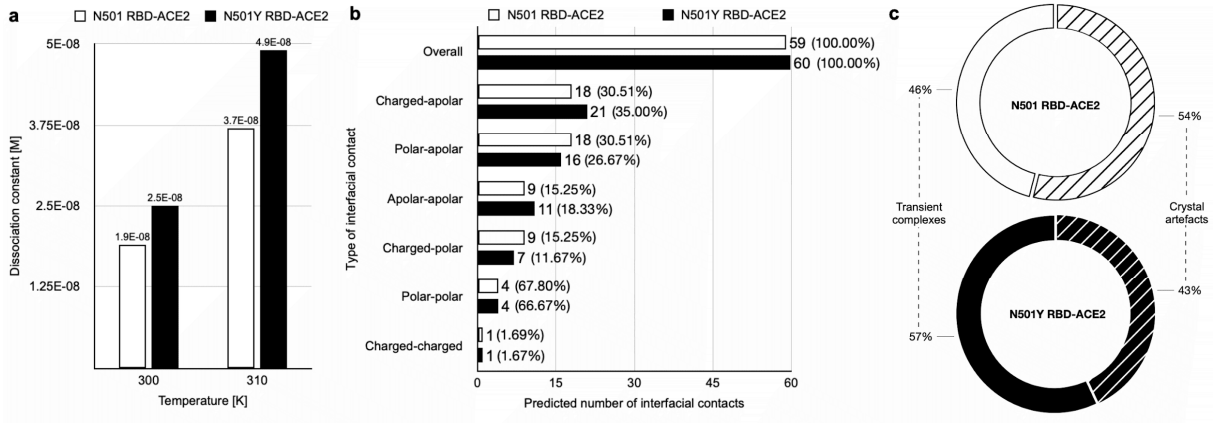

Figure S8. SwissADME's bioavailability radar for drug-likeness of the top ECR-ranked molecules. Drug-like compounds ideally are within the red range in the plots below.

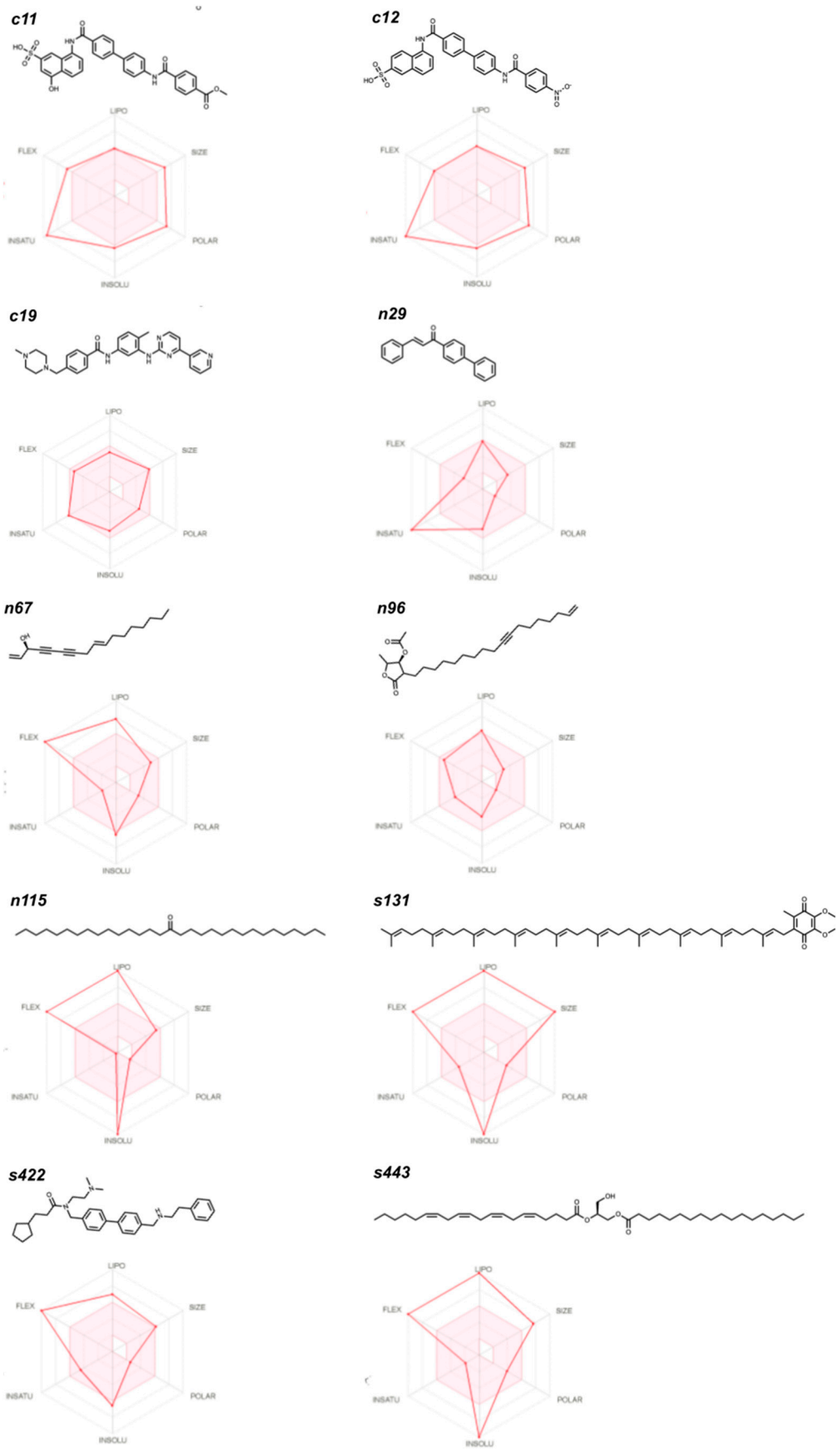

Figure S9. Associations between pathways and the studied compounds. The heatmap shows how likely a pathway (x-axis number-coded as in the PathwayMap server) is associated with a compound from a set (y-axis number-coded with the indexes assigned to the ligands). 1.0, Global and overview maps; 1.1, Carbohydrate metabolism; 1.2, Energy metabolism; 1.3, Lipid metabolism; 1.4, Nucleotide metabolism; 1.5, Amino acid metabolism; 1.6, Metabolism of other amino acids; 1.7, Glycan biosynthesis and metabolism; 1.8, Metabolism of cofactors and vitamins; 1.9, Metabolism of terpenoids and polyketides; 1.10, Biosynthesis of other secondary metabolites; 1.11, Xenobiotics biodegradation and metabolism; 2.1, Transcription; 2.2, Translation; 2.3, Folding, sorting and degradation; 2.4, Replication and repair; 3.1, Membrane transport; 3.2, Signal transduction; 3.3, Signaling molecules and interaction; 4.1, Transport and catabolism; 4.2, Cell growth and death; 4.3, Cellular community - eukaryotes; 4.5, Cell motility; 5.1, Immune system; 5.2, Endocrine system; 5.3, Circulatory system; 5.4, Digestive system; 5.5, Excretory system; 5.6, Nervous system; 5.7, Sensory system; 5.8, Development; 5.9, Aging; 5.10, Environmental adaptation; 6.1, Cancers: overview; 6.2, Cancers: specific types; 6.3, Immune diseases; 6.4, Neurodegenerative diseases; 6.5, Substance dependence; 6.6, Cardiovascular diseases; 6.7, Endocrine and metabolic diseases; 6.8, Infectious diseases: bacterial; 6.9, Infectious diseases: viral; 6.10, Infectious diseases: parasitic; 6.12, Drug resistance: antineoplastic. The server was able to run interactive pathway maps for 24 control (https://playmolecule.com/PathwayMap/job/D956706F), 124 natural (https://playmolecule.com/PathwayMap/job/9A3A9D46), and 489 synthetic (https://playmolecule.com/PathwayMap/job/61CE80A3#/) ligands.

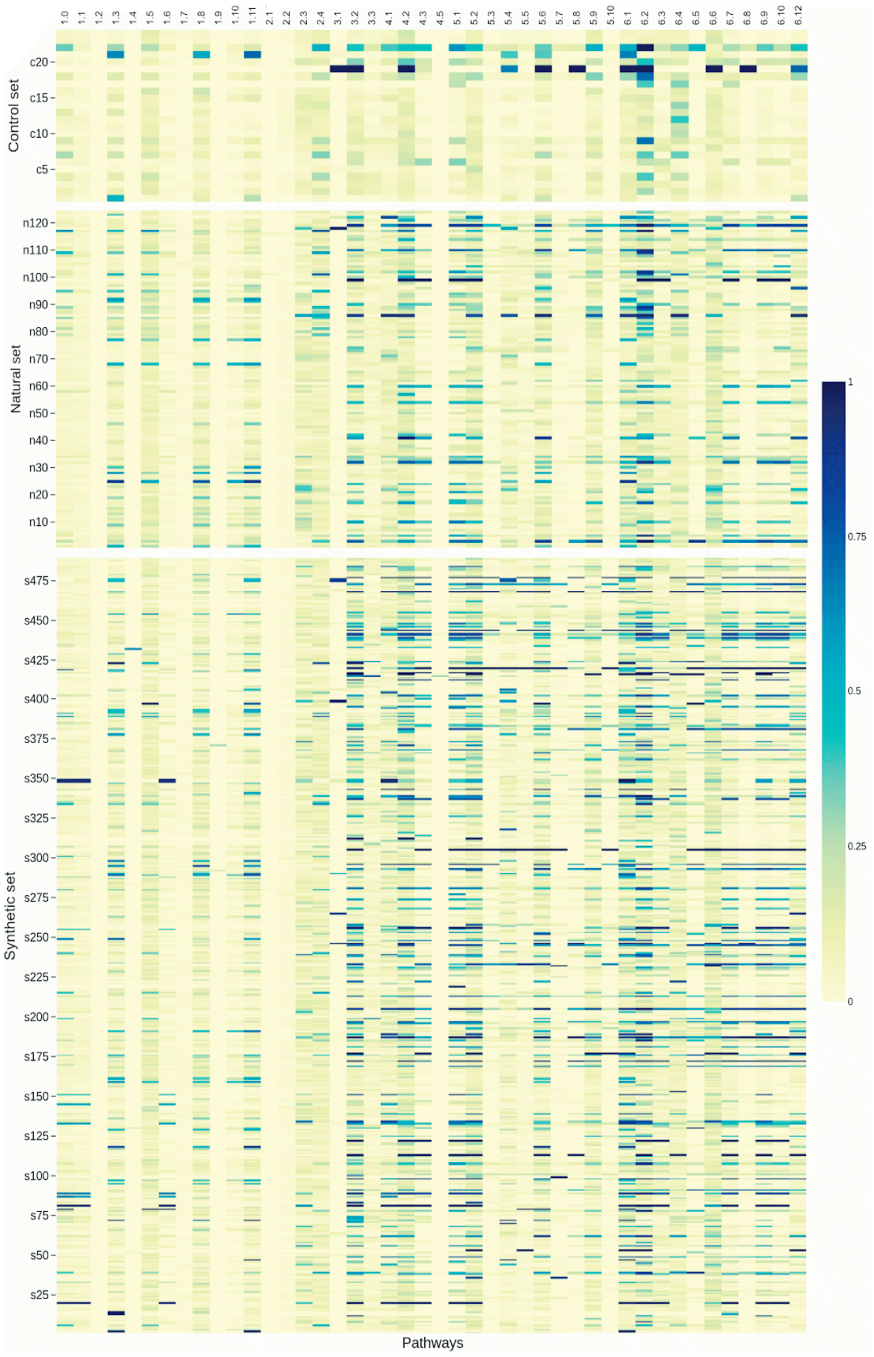

Figure S10. Overview of aligned wild-type (N501) RBDs. (a) 45º clockwise horizontal rotation of aligned 6M17, 6XE1 and 7JMP N501 RBDs in surface and (b) cartoon-only representations. (c) Comparison of N501 residues in each structure.

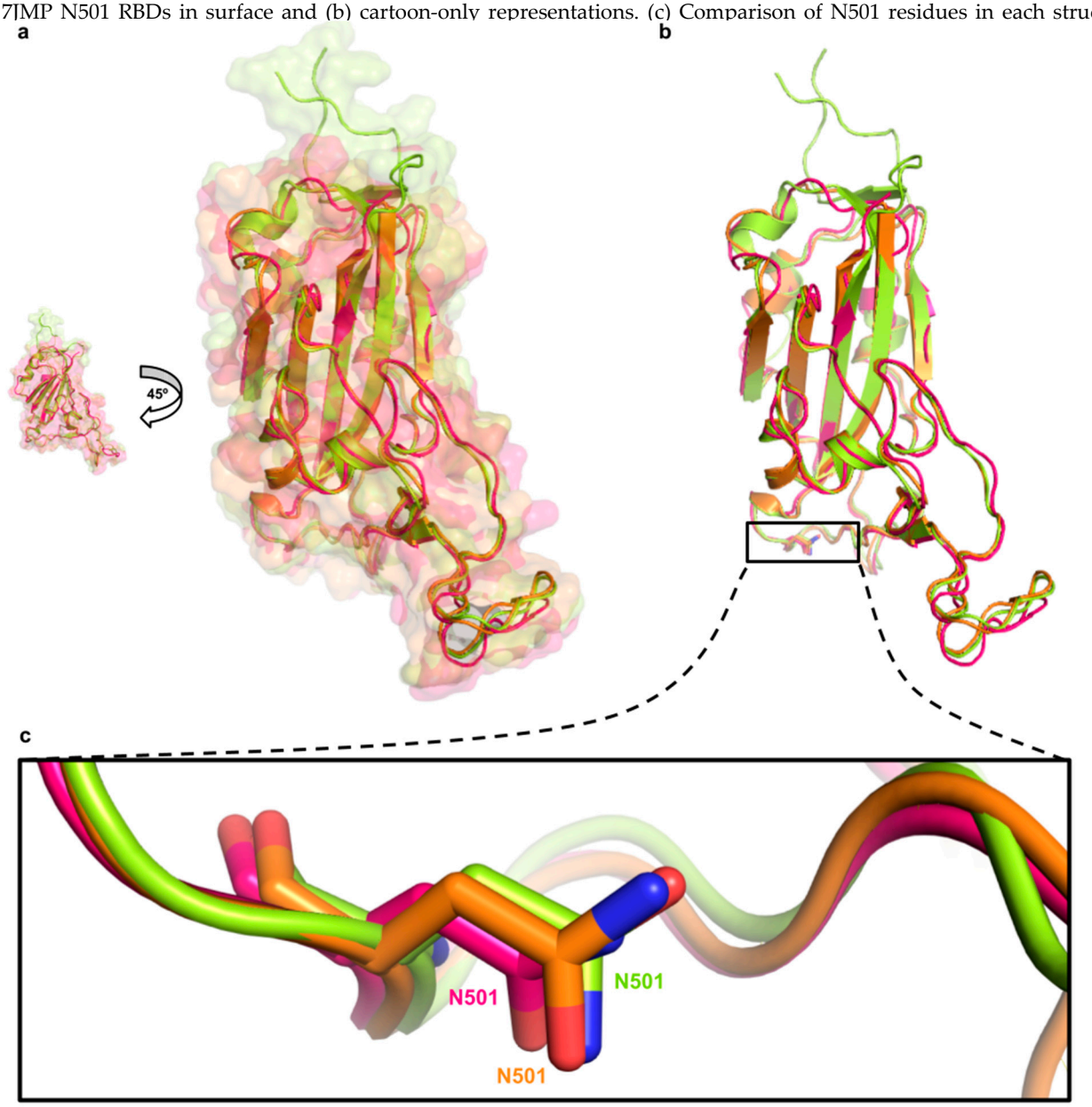

Figure S11. Overview of aligned and mutated (N501Y) RBDs. (a) surface and (b) cartoon-only representations of aligned 6M17, 6XE1, 7JMP N501Y RBDs (rotated 45º horizontally and clockwise as in Fig. 3. (c) N501Y comparison among RBDs. (d-f) Comparative between aligned 6M17 (d), 6XE1 (e) and 7JMP (f) N501 and N501Y RBDs.

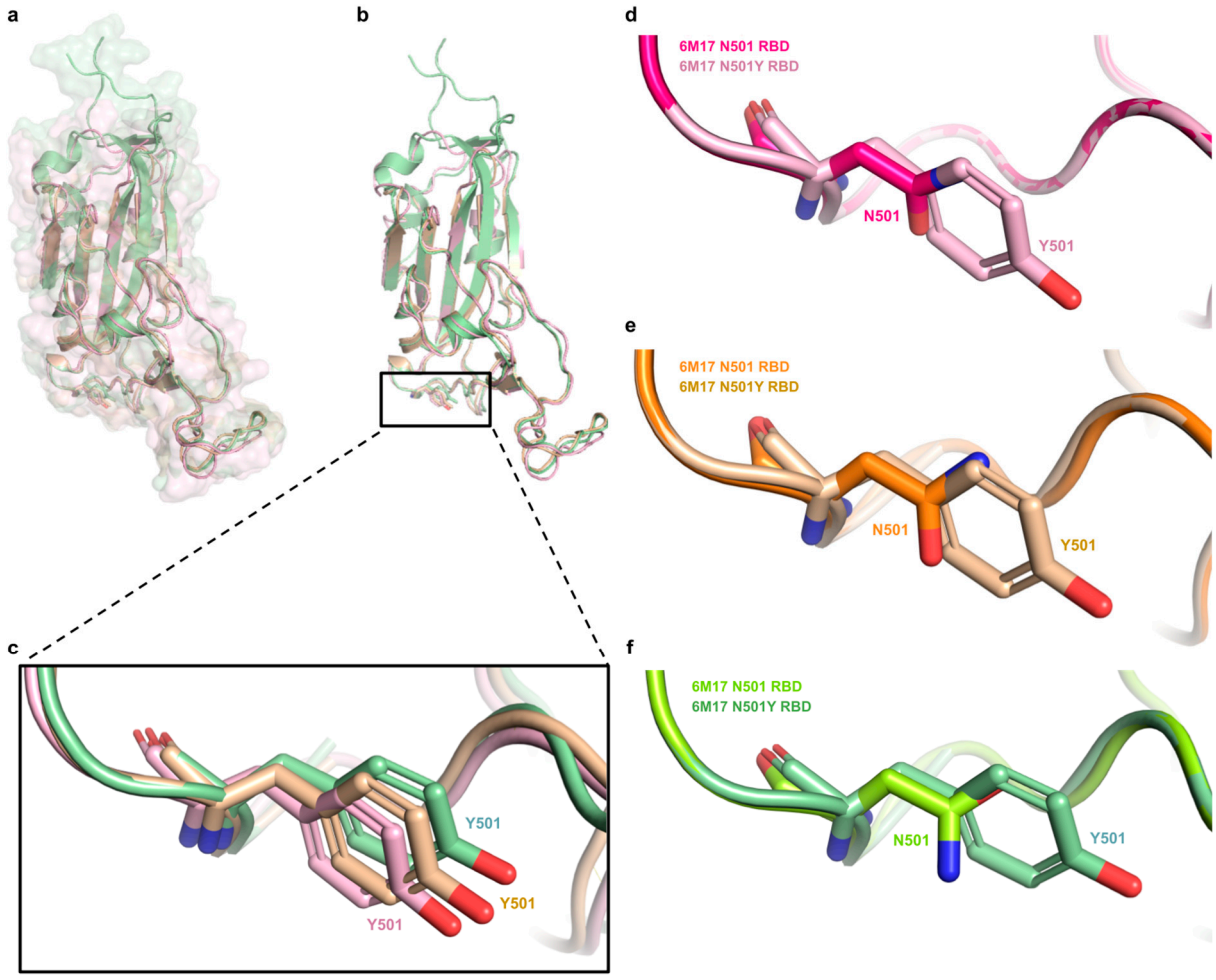

Supplementary Tables

Table S1. Docking sites and their key residues targeted for molecular docking. The two first columns indicate if a residue was considered in the wide and/or specific regions; the other columns refer to whether they were mentioned (black rectangle) or not (blank rectangle) by the listed authors (Supplementary Information)

Residues by region		ANDERSEN *et al.* (2020)	GULOTTA *et al.* (2020)	WU *et al.* (2020)	YAN *et al.* (2020)
Wide	**Specific**				
K417					
G446	G446		x	x	
Y449	Y449		x	x	
Y453			x	x	x
L455		x	x	x	x
F456			x	x	x
Q474			x		x
A475			x	x	
G476			x		
F486		x	x	x	x
N487			x	x	
Y489			x	x	
Q493		x	x	x	
S494		x			
G496	G496		x	x	
Q498	Q498		x	x	x
T500	T500		x	x	x
N501	N501	x	x	x	x
G502	G502		x	x	
Y505	Y505	x	x	x	

Table S2. Classification and IC_{50} values of the control dataset. The table contains all the control compounds used in the study. For cases where the same compound was assessed in studies under different stages (a preprint and a published paper), the IC_{50} value of the published article was stated.

Index	Classification	IC_{50} (μM)	Reference
c1	Inactive	> 1000	Fu *et al*., 2020
c2	Active	4.25	Bojadzic; Alcazar; Chen; Buchwald, 2020
c3	Active	113.2	Lin *et al*., 2020
c4	Active	2.57	Bojadzic; Alcazar; Chen; Buchwald, 2020
c5	Inactive	> 500	Bojadzic; Alcazar; Buchwald, 2020
c6	Active	0.99	Bojadzic; Alcazar; Chen; Buchwald, 2020
c7	Active	1.47	Bojadzic; Alcazar; Chen; Buchwald, 2020
c8	Active	39.2	Fu *et al*., 2020
c9	Active	0.16	Bojadzic; Alcazar; Chen; Buchwald, 2020
c10	Active	1.81	Bojadzic; Alcazar; Chen; Buchwald, 2020
c11	Active	4.04	Bojadzic; Alcazar; Chen; Buchwald, 2020
c12	Active	0.52	Bojadzic; Alcazar; Chen; Buchwald, 2020
c13	Active	3.35	Bojadzic; Alcazar; Chen; Buchwald, 2020
c14	Active	7.67	Bojadzic; Alcazar; Chen; Buchwald, 2020
c15	Active	9.95	Bojadzic; Alcazar; Chen; Buchwald, 2020
c16	Active	0.43	Bojadzic; Alcazar; Buchwald, 2020
c17	Active	2.25	Bojadzic; Alcazar; Chen; Buchwald, 2020
c18	Inactive	> 500	Bojadzic; Alcazar; Buchwald, 2020
c19	Active	0.13	Mulgaonkar *et al*., 2020
c20	Active	3.03	Bojadzic; Alcazar; Buchwald, 2020
c21	Inactive	Exact value unavailable	Fu *et al*., 2020
c22	Inactive	> 500	Bojadzic; Alcazar; Buchwald, 2020
c23	Active	8.7	Fu *et al*., 2020
c24	Active	0.4003	Fu *et al*., 2020

Table S3. RMSD values (Å) among the aligned RBD-containing structures. By default, the RBD-containing structures were aligned to 6M17 RBD, but other alignments are shown in the table above; RMSD values for the 6M17 complex were omitted since it had the same RBD as in 6M17 RBD.

RMSD		6M17		6XE1		7JMP	
		N501	N501Y	N501	N501Y	N501	N501Y
6M17	N501	0.000	0.000	0.821	0.831	0.852	0.855
	N501Y		0.000	0.820	0.821	0.852	0.853
6XE1	N501			0.000	0.001	0.372	0.375
	N501Y				0.000	0.373	0.372
7JMP	N501					0.000	0.000
	N501Y						0.000

Table S4. P-values for paired Wilcoxon two-tailed test to compare docking results according to RBD regions (wide ≠ specific) and versions (N501 ≠ N501Y). Wide and specific regions are compared to check for significant differences between their main docking results, according to each dataset and their RBD version (N501 or N501Y). Similarly, N501 and N501Y RBDs are compared, according to the datasets and their RBD regions (wide or specific).

RBD comparison	Dataset	RBD version or region	Chemscore	ΔG	ChemPLP
Wide and specific regions	Control	N501	1.94×10^{-5}	1.94×10^{-5}	1.37×10^{-4}
		N501Y	2.49×10^{-2}	8.22×10^{-3}	0.966
	Natural	N501	7.75×10^{-22}	2.52×10^{-21}	2.54×10^{-19}
		N501Y	2.29×10^{-20}	3.89×10^{-14}	4.38×10^{-22}
	Synthetic	N501	5.80×10^{-81}	2.92×10^{-73}	7.32×10^{-39}
		N501Y	1.16×10^{-77}	4.81×10^{-61}	2.24×10^{-47}
N501 and N501Y	Control	Wide	5.28×10^{-5}	1.93×10^{-3}	4.09×10^{-3}
		Specific	1.94×10^{-5}	2.51×10^{-5}	2.21×10^{-5}
	Natural	Wide	1.89×10^{-19}	8.78×10^{-17}	5.33×10^{-15}
		Specific	5.32×10^{-22}	2.11×10^{-21}	2.74×10^{-18}
	Synthetic	Wide	9.21×10^{-69}	1.07×10^{-52}	2.26×10^{-52}
		Specific	4.06×10^{-76}	4.63×10^{-70}	6.46×10^{-40}

Table S5. P-values for paired Wilcoxon one-tailed test to compare docking results in RBD regions (wide > specific) and versions (N501 > N501Y). Docking regions are compared to check whether the wide region has significantly superior docking results, according to each dataset and their RBD version (N501 or N501Y). Similarly, RBD versions are compared, checking whether the N501 region has significantly better results than N501Y RBDs, according to the datasets and their RBD regions (wide or specific). Since the higher the Chemscore and ChemPLP scores and the lower the ΔG values, the more favorable the results, ΔG values were multiplied by −1 to be correctly interpreted in the Python program.

RBD comparison	Dataset	RBD version or region	Chemscore	ΔG	ChemPLP
Wide and specific regions	Control	N501	9.71×10^{-6}	9.70×10^{-6}	6.83×10^{-5}
		N501Y	1.25×10^{-2}	4.11×10^{-3}	0.483
	Natural	N501	3.88×10^{-22}	1.26×10^{-21}	1.27×10^{-19}
		N501Y	1.15×10^{-20}	1.95×10^{-14}	2.19×10^{-22}
	Synthetic	N501	2.90×10^{-81}	1.46×10^{-73}	1.00
		N501Y	5.80×10^{-78}	2.40×10^{-61}	1.12×10^{-47}
N501 and N501Y	Control	Wide	1.00	1.00	1.00
		Specific	1.00	1.00	1.00
	Natural	Wide	1.00	1.00	1.00
		Specific	1.00	1.00	1.37×10^{-18}
	Synthetic	Wide	1.00	1.00	1.00
		Specific	1.00	1.00	3.23×10^{-40}

Table S6. *P*-values for paired Wilcoxon one-tailed test to compare docking results in RBD regions (wide < specific) and versions (N501 < N501Y). P-values for paired Wilcoxon one-tailed test to compare docking results in RBD regions (wide < specific) and versions (N501 < N501Y). Docking regions are compared to check whether the wide region has significantly inferior docking results, according to each dataset and their RBD version (N501 or N501Y). Similarly, RBD versions are compared, checking whether the N501 region has significantly worse results than N501Y RBDs, according to the datasets and their RBD regions (wide or specific). Since the higher the Chemscore and ChemPLP scores and the lower the ΔG values, the more favorable the results, ΔG values were multiplied by −1 to be correctly interpreted in the Python program.

RBD comparison	Dataset	RBD version or region	Chemscore	ΔG	ChemPLP
Wide and specific regions	Control	N501	1.00	1.00	1.00
		N501Y	0.988	0.996	0.528
	Natural	N501	1.00	1.00	1.00
		N501Y	1.00	1.00	1.00
	Synthetic	N501	1.00	1.00	3.66×10^{-39}
		N501Y	1.00	1.00	1.00
N501 and N501	Control	Wide	2.64×10^{-5}	9.67×10^{-4}	2.04×10^{-3}
		Specific	9.70×10^{-6}	1.25×10^{-5}	1.10×10^{-5}
	Natural	Wide	9.43×10^{-20}	4.39×10^{-17}	2.66×10^{-15}
		Specific	2.66×10^{-22}	1.05×10^{-21}	1.00
	Synthetic	Wide	4.60×10^{-69}	5.36×10^{-53}	1.13×10^{-52}
		Specific	2.03×10^{-76}	2.31×10^{-70}	1.00

Table S7. Top 10 ranked molecules in docking simulations. Their IUPAC or common names (when applicable) are indicated below.

c11	4-hydroxy-8-(4'-(4-(methoxycarbonyl)benzamide)-[1,1'-biphenyl]-4-carboxamide)naphthalene-2-sulfonic acid (DRI-C2204745)
c12	5-(4'-(4-nitrobenzamide)-[1,1'-biphenyl]-4-carboxamido)naphthalene-2-sulfonic acid (DRI-C23041)
c19	4-[(4-methylpiperazin-1-yl)methyl]-N-[4-methyl-3-[(4-pyridin-3-ylpyrimidin-2-yl)amino]phenyl]benzamide (imatinib)
n29	(*E*)-3-phenyl-1-(4-phenylphenyl)prop-2-en-1-one
n67	2-methyl-4-(octadec-17-en-10-yn-1-yl)-5-oxotetrahydrofuran-3-yl acetate
n96	(9*E*)-heptadeca-1,9-dien-4,6-diyn-3-ol (falcarinol)
n115	hentriacontane-16-one (palmitone)
s131	2-[(2*E*,6*E*,10*E*,14*E*,18*E*,22*E*,26*E*,30*E*,34*E*)-3,7,11,15,19,23,27,31,35,39-decamethyltetraconta-2,6,10,14,18,22,26,30,34,38-decaenyl]-5,6-dimethoxy-3-methylcyclohexa-2,5-diene-1,4-dione (coenzyme Q10)
s422	3-cyclopentyl-N-[2-(dimethylamino)ethyl]-N-[[4-[4-[(2-phenylethylamino)methyl]phenyl]phenyl]methyl]propanamide (SB-699551)
s443	(1-hydroxy-3-octadecanoyloxypropan-2-yl) (5*Z*,8*Z*,11*Z*,14*Z*)-icosa-5,8,11,14-tetraenoate (1-stearoyl-2-arachidonoylglycerol)

Table S8. Comparison of N501 and N501Y RBD-ACE2 complexes by PDBePISA. In these circumstances, the solvation energies displayed by PDBePISA should not be considered in absolute values, because the structures analyzed contain the RBD, but not entirely the Spike protein, to which a portion of the RBD would be attached and not exposed (as well as a part of ACE2, since it is a transmembrane protein). Instead, they should be interpreted qualitatively, comparing two RBDs differing in one residue.

Evaluation		**N501 RBD-ACE2 complex**		**N501Y RBD-ACE2 complex**	
		RBD	**ACE2**	**RBD**	**ACE2**
Interface	Atoms	95	107	87	90
	Residues	27	27	25	24
	Solvent-accessible area [Å^2]	961.2	901.6	838.9	810.6
Solvation energy [kJ mol^{-1}]	Isolated structure	–701.7	–3,319.2	–637.6	–3,053.1
	Gain on complex formation	–4.2	7.1	–12.1	0.84
	Average gain	–8.8	–3.3	–12.6	–9.2

Table S9. Confidence intervals of eMolTox for top ECR-ranked molecules. ADMET properties predicted by eMolTox for a molecule for a 0.05 significance level α. Each value represents a confidence interval for an ADMET property of a ligand, which can present either a positive or negative result. Red indicates a concerning characteristic (e.g., positive result as a disruptor of the mitochondrial membrane potential); blue, optimal (e.g., negative result for liver injury); yellow, requiring further analysis; zero values indicate that it wasn't able to return a given property for a particular ligand with α ≤ 0.05. Also, the yellow color for compounds acting as modulators doesn't necessarily infer (a) toxicity, but the risk of a compound losing its potential specificity against RBD if it can act as a modulator of other targets. All the ten ligands had negative results as modulators of cyclooxygenase-2, beta (2 and 3) adrenergic receptors, vascular endothelial growth factor receptors (1 and 2), dopamine D1 receptor, calcitonin gene-related peptide type 1 receptor, receptor protein-tyrosine kinase erbB-2, adenosine A2a receptor, dopamine D2 receptor, glutamate NMDA receptor, androgen receptor, dopamine transporter, serotonin 3a (5-HT3a) receptor, histamine H1 receptor, melatonin receptor 1B, adenosine A2b receptor, beta-1 adrenergic receptor, serotonin 4 (5-HT4) receptor, alpha-1a adrenergic receptor, sigma opioid receptor, adenosine A3 receptor, peroxisome proliferator-activated receptor gamma, delta-opioid receptor, sodium channel protein type IX alpha subunit, norepinephrine transporter, P2X purinoceptor (3 and 7), adenosine A1 receptor, endothelin receptor ET-B, vascular endothelial growth factor receptor and serotonin 7 (5-HT7) receptor, endothelin receptor ET-A.

	c11	*c12*	*c19*	*n29*	*n67*	*n96*	*n115*	*s131*	*s422*	*s443*
BSEP inhibitor	0.970 (–)	0.970 (–)	0.988 (+)	0.000	0.000	0.000	0.000	0.000	0.976 (+)	0.000
Cytotoxicity in HepG2 cells (8 h)	0.981 (+)	0.981 (+)	0.000	0.000	0.000	0.000	0.964 (+)	0.000	0.956 (+)	0.000
Cytotoxicity in HepG2 cells (16 h)	0.983 (+)	0.983 (+)	0.000	0.000	0.000	0.000	0.971 (+)	0.000	0.978 (+)	0.000
Cytotoxicity in HepG2 cells (24 h)	0.970 (+)	0.970 (+)	0.000	0.000	0.000	0.000	0.000	0.000	0.981 (+)	0.000
Cytotoxicity in HepG2 cells (32 h)	0.951 (+)	0.951 (+)	0.976 (+)	0.000	0.000	0.000	0.000	0.000	0.965 (+)	0.000
Cytotoxicity in HepG2 cells (40 h)	0.000	0.000	0.984 (+)	0.000	0.000	0.000	0.000	0.000	0.994 (+)	0.000
Cytotoxicity in HEK293 cells (8 h)	0.989 (+)	0.990 (+)	0.000	0.000	0.000	0.951 (+)	0.980 (+)	0.000	0.963 (+)	0.000
Cytotoxicity in HEK293 cells (16 h)	0.988 (+)	0.988 (+)	0.000	0.000	0.000	0.000	0.974 (+)	0.000	0.000	0.000
Cytotoxicity in HEK293 cells (24 h)	0.975 (+)	0.975 (+)	0.000	0.000	0.000	0.962 (+)	0.972 (+)	0.000	0.981 (+)	0.000
Cytotoxicity in HEK293 cells (32 h)	0.965 (+)	0.966 (+)	0.000	0.000	0.000	0.000	0.968 (+)	0.000	0.960 (+)	0.000
Cytotoxicity in HEK293 cells (40 h)	0.000	0.000	0.000	0.000	0.000	0.959 (+)	0.958 (+)	0.000	0.982 (+)	0.000
Induce genotoxicity in human embryonic kidney cells	0.971 (+)	0.971 (+)	0.000	0.983 (+)	0.969 (–)	0.981 (–)	0.973 (–)	0.000	0.000	0.979 (–)
Liver injury	0.966 (+)	0.966 (+)	0.996 (+)	0.000	0.000	0.979 (–)	0.976 (–)	0.000	0.000	0.975 (–)
Modulator of angiotensin-converting enzyme	0.997 (–)	0.997 (–)	0.993 (–)	0.992 (–)	0.993 (–)	0.993 (–)	0.996 (–)	0.993 (–)	0.996 (–)	1.000 (–)
Modulator of angiotensin II type 1 receptor	0.993 (–)	0.994 (–)	0.989 (–)	0.996 (–)	0.996 (–)	0.993 (–)	0.999 (–)	1.000 (–)	0.992 (–)	0.996 (–)
Modulator of angiotensin II type 2 receptor	0.996 (–)	0.989 (–)	0.985 (–)	0.989 (–)	0.997 (–)	0.997 (–)	0.985 (–)	0.000	0.980 (–)	0.971 (–)
Modulator of muscarinic acetylcholine receptor M2	0.983 (–)	0.983 (–)	0.999 (–)	0.999 (–)	(+) 0.951	0.997 (–)	(+) 0.986	(+) 0.965	(+) 0.969	(+) 0.994
Modulator of Glucocorticoid receptor	0.999 (–)	0.999 (–)	0.999 (–)	0.996 (–)	0.997 (–)	0.998 (–)	0.993 (–)	0.000	0.995 (–)	0.995 (–)
Modulator of Platelet activating factor receptor	0.987 (–)	0.996 (–)	0.982 (+)	0.990 (–)	0.972 (–)	0.996 (–)	0.983 (–)	0.964 (–)	0.973 (+)	0.970 (–)
Modulator of Serotonin 2c (5-HT2c) receptor	0.996 (–)	0.996 (–)	0.993 (–)	0.992 (–)	0.992 (–)	0.995 (–)	0.989 (–)	0.993 (–)	0.990 (+)	0.997 (–)
Modulator of Alpha-1b adrenergic receptor	0.993 (–)	0.995 (–)	0.997 (–)	0.996 (–)	0.999 (–)	0.996 (–)	0.993 (–)	0.982 (–)	0.988 (+)	0.999 (–)
Modulator of Muscarinic	0.959 (–)	0.967 (–)	0.991 (–)	0.966 (–)	0.959 (+)	0.965 (–)	0.988 (+)	0.987 (+)	0.960 (–)	0.988 (+)

acetylcholine receptor M4										
Modulator of Serotonin 1b (5-HT1b) receptor	0.973 (–)	0.974 (–)	0.972 (+)	0.986 (–)	0.978 (–)	0.967 (–)	0.957 (–)	0.969 (–)	0.994 (+)	0.982 (–)
Modulator of Muscarinic acetylcholine receptor M3	0.974 (–)	0.974 (–)	0.999 (–)	0.994 (–)	0.961 (–)	0.976 (–)	0.978 (+)	0.962 (+)	0.981 (+)	0.973 (+)
Modulator of Serotonin 1a (5-HT1a) receptor	0.993 (–)	0.992 (–)	0.988 (–)	0.999 (–)	1.000 (–)	1.000 (–)	0.995 (–)	0.994 (–)	0.984 (+)	1.000 (–)
Modulator of Serotonin 2a (5-HT2a) receptor	0.985 (–)	0.984 (–)	0.987 (+)	0.994 (–)	0.991 (–)	0.983 (–)	0.984 (–)	0.985 (–)	0.994 (+)	0.997 (+)
Modulator of Acetylcholinesterase	0.967 (+)	0.967 (+)	0.992 (–)	0.999 (–)	0.981 (–)	0.992 (–)	0.974 (–)	0.000	0.982 (+)	0.961 (+)
Modulator of HERG	0.987 (–)	0.987 (–)	0.978 (–)	0.978 (–)	0.968 (–)	0.968 (–)	0.000	0.000	0.973 (+)	0.975 (–)
PDGFRA modulator	(–) 0.976	(–) 0.974	(+) 0.999	(–) 0.970	(–) 0.983	(–) 0.980	(–) 0.975	(–) 0.970	(–) 0.979	(–) 0.978
PDGFRB modulator	(–) 0.981	(–) 0.981	(+) 0.999	(–) 0.984	(–) 0.986	(–) 0.996	(–) 0.989	(–) 0.978	(–) 0.969	(–) 0.982

Supplementary Methods

Free energy calculations

Once molecular dynamics simulations and sub-trajectories with the highest stability were obtained, we estimated the binding free energy from MM-GBSA (Molecular mechanics with generalized Born and surface area solvation)[60,61]. Amber18 was used to perform MM-GBSA calculations (equation 1)

$$\Delta G = G_C - G_R - G_I \quad (1)$$

where G_C is the energy of the complex, G_R is the energy of the receptor and G_I describes the energy of the inhibitor. Frames from 1 to 500 of the most stable sub-trajectories were used (for all cases, the 150 ns trajectories were used). Applying this method made it possible to estimate the binding free energy of the complexes formed between RBD (with and without the N501Y mutation) and the candidate inhibitors under study.

Free energy decomposition

The free energy values were calculated from the residues' decomposition to understand better the interaction between amino acid residues (equation 2) and the compounds under study.

$$\Delta G_{I_R} = \Delta G_{vdW} - \Delta G_{Ele} - \Delta G_{GB} \quad (2)$$

ΔG_{I_R} is the free energy of amino acid residues; ΔG_{vdW} is the energy of van der Waals; ΔG_{Ele} is the electrostatic energy and ΔG_{GB} is the energy of solvation calculated from the generalized Born method. This approximation was performed using the Amber18 program, with a molarity concentration of 0.100 M. The results were used to evaluate the energy behavior of RBD residues in the presence of the potential inhibitors.

Supplementary Discussion

H bonds and hydrophobic interactions in the protein-ligand complexes

Interactions involving various tyrosine residues were found between RBD-containing structures and the selected hits. The most frequent interacting residue was Y489, establishing H bonds and predominating hydrophobic contact, particularly for the N501 RBD-containing structures. However, the overall number of interactions was slightly higher in N501Y RBDs, which is worth highlighting Y505 hydrophobic contacts and S494 H bonds. When comparing the total number of interactions of residue 501 among RBD N501 and N501Y RBD-containing structures, the quantity increased more than 9-fold from the former to the latter. In addition, N501 did not interact via hydrophobic interactions, whereas Y501 did, besides interacting through H bonds.

ACE2 interacted hydrophobically with the hits mainly through phenylalanine and leucine residues, and through H bonds by glutamines. F28 was the most frequent residue of ACE2, forming more hydrophobic contacts with the hits when complexed with N501Y RBD. Most interactions were hydrophobic, and their proportions were equal between ACE2s complexed with N501 or N501Y RBDs, albeit the absolute number of interactions by the main interacting residues increased in N501Y RBD-ACE2. In addition, E35 H bonds were absent in N501 RBD-ACE2 but prevailed in N501Y RBD-ACE2, whereas the Q76 H bond was not identified anymore (Fig. S6).

H bonds and hydrophobic interactions in the RBD-ACE2 complexes

From the PDBePISA server, the solvent-accessible interface area for RBD-ACE2 was found to be smaller in N501Y than in N501 RBD. Despite that, we can note interesting issues: (1) residues labeled as inaccessible become accessible; (2) the solvation energy gain related to the complex formation and its average gain become more favorable in the complex with the mutated RBD (Table S7); (3) concomitantly, Y501 presented 59.11% more accessible surface area (ASA, a total of 72.19 $Å^2$) and 76.82% extra buried surface area (BSA, 65.00 $Å^2$ in total) than N501. A larger residue ASA could increase RBD-ACE2 interactions; a greater BSA could support immune evasion.

The shortest H bond distance at the RBD-ACE2 complex, identified in the server, was 2.58 Å for the O atom in Y489 (RBD) and OH in E27 (ACE2) N501 and N501Y RBDs. Y489 was substantially involved in H bonds and hydrophobic protein-ligand interactions. In addition, nine H bonds between N501 RBD and ACE2 were observed, while eight were found between N501Y RBD and ACE2; the H bond detected between N501 and Y41 was not found between Y501 and ACE2 atoms. However, from the structure visualization using PyMOL, nine protein-protein polar contacts were observed in both RBD versions complexed with ACE2 — including Y501 and K353 in the mutated case, forming H bonds with 1.77 and 2.38 Å of distance, respectively, whereas an H bond between N501 and K353 was also detected (2.33 Å) (Fig. S7).

From the PRODIGY server, we assessed the estimated free energy changes (ΔG) and the dissociation constants (k_d) for N501 and N501Y RBDs complexed with ACE2. ΔG values were considerably similar (–43.93 and –43.51 kJ mol^{-1}, respectively); k_d was smaller for N501Y RBD-ACE2. This suggests that the complex formation remained energetically favorable, with the faster association and slower dissociation rates between RBD-ACE2.

The overall predicted number of interfacial contacts was similar, but N501Y RBD-ACE2 had an extra interfacial contact; per property, charged-apolar and apolar-apolar interactions prevailed in both but increased in N501Y RBD-ACE2. However, from N501 to N501Y RBD-ACE2, there were fewer charged-polar and polar-polar contacts, whereas the charged-charged and polar-polar contacts remained constant. Thus, there was an increase in apolar-related contacts and a decrease in polar-related ones.

The HyPPI Prediction server gave us the proportions of transient complexes to crystal artifacts for N501 and N501Y RBD-ACE2 complexes. Notably, there was an increase in the stabilization of the N501Y RBD-ACE2 transient complex, which implies more biologically relevant interactions (Fig. S8).

Supplementary Notes

The following calculations were performed to quantify the total number of docking poses:

8 structures × 2 sites × 637 compounds × 100 runs = 1,019,200 poses.

8 structures × most promising site × 10 hits × 25 repetitions × 100 runs = 200,000 poses.

Summing the number of docking poses above, 1,219,200 poses were generated.

Additionally, ten other ligands were evaluated after this study, resulting in a total of 1,235,200 poses, but such molecules were not further investigated since they did not surpass the other top-scoring compounds.

Supplementary References

57. Fu, W.; Chen, Y.; Wang, K.; Hettinghouse, A.; Hu, W.; Wang, J.-Q.; Lei, Z.-N.; Chen, Z.-S.; Stapleford, K.A.; Liu, C-J. Repurposing FDA-approved drugs for SARS-CoV-2 through an ELISA-based screening for the inhibition of RBD/ACE2 interaction. *Protein Cell* **2021**, *12*, 586–591.
58. Bojadzic, D.; Alcazar, O.; Buchwald, P. Methylene Blue Inhibits the SARS-CoV-2 spike–ACE2 Protein-Protein Interaction–a Mechanism that can Contribute to its Antiviral Activity Against COVID-19. *Frontiers in Pharmacology* **2021**, *11*, 600372.
59. Lin, C.; Li, Y.; Zhang, Y.; Liu, Z.; Mu, X.; Gu, C.; Liu, J.; Li, Y.; Li, G.; Chen, J. Ceftazidime Is a Potential Drug to Inhibit SARS-CoV-2 Infection In Vitro by Blocking Spike Protein-ACE2 Interaction. Available online: https://biorxiv.org/content/10.1101/2020.09.14.295956v1.full (accessed on 20 February 2021).
60. Mulgaonkar, N.S.; Wang, H.; Mallawarachchi, S.; Růžek, D.; Martina, B.; Fernando, S. Bcr-Abl Tyrosine Kinase Inhibitor Imatinib as a Potential Drug for COVID-19. Available online: https://biorxiv.org/content/10.1101/2020.06.18.158196v2 (accessed on 20 February 2021).
61. Bojadzic, D.; Alcazar, O.; Chen, J.; Buchwald, P. Small-Molecule In Vitro Inhibitors of the Coronavirus Spike-ACE2 Protein-Protein Interaction as Blockers of Viral Attachment and Entry for SARS-CoV-2. Available online: https://biorxiv.org/content/10.1101/2020.10.22.351056v1 (accessed on 20 February 2021).
62. Virtanen; Salla, I.; Niinivehmas, S.P.; Pentikäinen, O.T. Case-specific performance of MM-PBSA, MM-GBSA, and SIE in virtual screening. *J. Mol. Graph. Model.* **2015**, *62*, 303–318.
63. Wang, E.; Sun, H.; Wang, J.; Wang, Z.; Liu, H.; Zhang, J.Z.; Hou, T. End-point binding free energy calculation with MM/PBSA and MM/GBSA: Strategies and applications in drug design. *Chem. Rev.* **2019**, *119*, 9478–9508.